Magnetic Determination of Axial Catalyst Temperature Profiles

A magnetic thermometric method is used to determine cross-sectional average axial catalyst temperature profiles for superparamagnetic nickel catalyst beds during ethane hydrogenolysis, an exothermic reaction. Each solid temperature profile is determined from an axial profile of cross-sectional average magnetization and is represented by a polynomial. In turn, each magnetization profile is determined from voltage data obtained as the bed is moved through an AC permeameter. A Fredholm equation of the first kind, "regularized" using a minimum variance constraint, is inverted to determine the magnetization profile.

The determination of the axial temperature profile for a reactor operating at 11.0% conversion is detailed. It provides a good test of the method used. Some limitations of the method are highlighted by attempts to analyze data from a reactor operating at complete conversion. The potential for model parameter estimation is discussed.

T. S. Cale
J. A. Merson
Chemical, Bio & Materials Eng. Dept.
Center for Energy Systems Research
Arizona State University
Tempe, AZ 85287

Introduction

Catalyst temperature is of fundamental importance in heterogeneous catalytic kinetics, reactor design, and reactor operation. Though the local catalyst-phase temperature is determined largely by the local fluid conditions, the detailed relationship between the properties of each phase and between catalyst pellets has not been experimentally verified through measurements of catalyst temperature. Thus, measurements of catalyst temperatures are important to the validation of current and future heterogeneous reactor models. Until recently, experimental information regarding the temperature of practical catalysts during use was limited to thermocouple-obtained temperatures of single catalyst pellets (Kehoe and Butt, 1972) or individual pellets in a bed (Balakrishnan and Pei, 1979). Though interesting in their own right, comparing the measured temperatures with heterogeneous model predictions provides limited insight. Even in the latter case, conduction of the thermocouple and thermocouple well will modify their thermal environment and change the measurement to some ill-defined average temperature. In addition, this technique is not feasible for the small catalyst particles common in laboratory kinetic studies.

Recently, Cale (1984) and Cale and Ludlow (1984a, b) developed a magnetic thermometric technique to measure the well-defined volume-average solid temperature of a bed of supported nickel catalyst during ethane hydrogenolysis. The technique uses the temperature dependence of the magnetic moment density (magnetization) of superparamagnetic nickel catalysts. Superparamagnetic samples behave like paramagnetic samples; however, their particle moments are much larger (Selwood, 1975). Data obtained at low magnetic field intensities are sufficient to determine changes in magnetization of these superparamagnetic samples (Cale et al., 1983). An AC permeameter (ACP), a low field induction device with an output voltage which is linear in sample magnetic moment, is used to follow changes in sample magnetization (Selwood, 1975; Cale and Ludlow, 1984b). The primary coil of the ACP shown schematically in Figure 1 surrounds two well-balanced secondary coils connected in series opposition. The catalyst sample is centered in the ACP secondary coil whose output voltage increases with sample magnetic moment. The net RMS output voltage of the secondary coils is followed during process changes. For example, if ethane hydrogenolysis is initiated by introducing ethane into a stream of hydrogen and perhaps helium flowing through the catalyst bed, the catalyst temperature increases due to the exothermic nature of the reaction. The average solid temperature rise is calculated from the decrease in ACP voltage using a calibration which relates the change in voltage directly to the change in sample temperature (Cale, 1984). The decrease in hydrogen partial pressure upon starting the flow of ethane tends to increase the sample magnetization due to desorption (Selwood, 1975; Cale, 1984), acting against the effect of tempera-

Correspondence concerning this paper should be addressed to T. S. Cale.

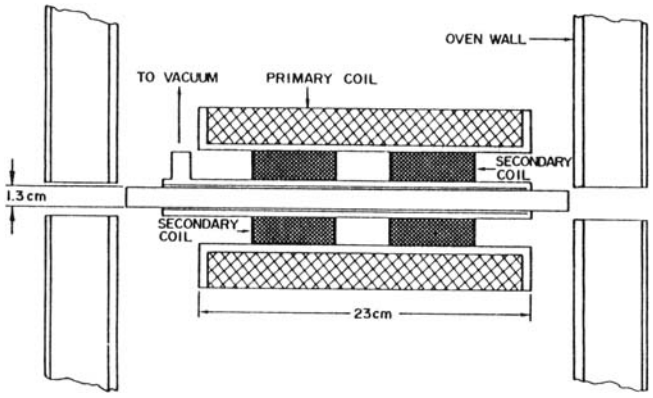

Figure 1. ACP used to determine the bed-average catalyst temperature.

ture change. To account for the desorption of hydrogen, the decrease in voltage observed in the thermometry is increased in magnitude using a calibration relating the change in hydrogen partial pressure to the change in ACP voltage (Cale, 1984; Ludlow, 1986). The converse analysis is used if a thermometry experiment is performed upon reaction termination.

One conclusion from the thermometric experiments is that the local time-average crystallite temperature is the same as the local support temperature. This conclusion supports theoretical calculations (Luss, 1970; Steinbruchel and Schmidt, 1973; Holstein and Boudart, 1983), and the same conclusion has been derived from more recent experimental results (Sharma et al., 1988). Thus, the technique measures the bed average catalyst temperature that would be calculated by averaging over the solid phase, which is an experimental property not previously available. The measurements allow new studies with heterogeneous reactor models, since the average solid temperatures predicted by the models are easily computed. The method has been used to determine the interphase heat transfer coefficients in packed-bed reactors operated at low conversion (Cale and Lawson, 1985) within the differential reactor assumption. The behavior of single catalyst pellets has also been studied (Cale, 1988). While data obtained using the method have proven useful in studies of more complete reactor models (Cale et al., 1987), it is more desirable to have the cross-sectional average catalyst temperature at each axial bed position.

This paper reports on the extension of the bed average magnetic crystallite thermometry to determine axial nickel catalyst temperature profiles during ethane hydrogenolysis. The basic limitations of the thermometry are the same as for the bed average thermometry, and the experimental equipment is similar. For temperature profile determinations, data are gathered as the bed, operating at steady state, is moved relative to the ACP secondary coils. The technique is an extension of that used by Richardson (1971) to determine the amount of sulfur adsorbed as a function of axial position in a packed bed of nickel adsorbent. The cross-sectional average magnetization of the catalyst is determined by inverting the Fredholm equation of the first kind which arises from theory. The cross-sectional average catalyst temperature profile is calculated from the magnetization profile using calibrations. The calibrations between magnetization and catalyst temperature and between magnetization and hydrogen partial pressure are obtained in the same way as for the bed average thermometry. Their use is somewhat different for profile determination, since changes in ACP voltage cannot be related directly to local temperature and hydrogen pressure changes. (See the Calibrations section.)

The determination of the axial catalyst temperature profile of a bed operating at 11.0% conversion of ethane is detailed. Because of the low flow rate and presence of axial dispersion, this example provides a good test of the extension of the magnetic thermometric method to profile determinations. Some limitations of the technique, as it is currently used, are highlighted by attempts to study a bed operating at complete conversion.

Theory

The determination of catalyst temperature profiles requires the measurement of the output voltage of an ACP as a function of the position of the sample in the ACP. Figure 2 shows the configuration of the sample, reactor and AC permeameter used to determine the temperature profiles reported in this work. It also introduces some of the nomenclature. The position of the catalyst bed in the ACP (X in Figure 2) is specified by using the outlet face of the bed as a reference point. The position within the bed is measured relative to this reference point (ξ in Figure 2). The position of magnetic material is specified by X and ξ. From Faraday's law, the instantaneous voltage (E) induced in the secondary coils of the ACP, due to the magnetic catalyst sample, is the integral, over the bed length, of the local rate of change in magnetization (I) times local coil sensitivity (Hayt, 1974):

$$E(X, t) = \int_0^{\ell} \sigma(X + \xi) \frac{\partial I(X, \xi, t)}{\partial t} d\xi \qquad (1)$$

where ℓ is the length of the bed. The sensitivity $\sigma(X + \xi)$ is the output voltage of the *entire* ACP per unit rate of magnetization change at position $X + \xi$ in the ACP (see Figure 2). It depends on the number of loops in the coil and the coil geometry and is determined as a function of X from experiment. Thus, the voltage induced due to the catalyst depends on the position of the bed in the ACP. The changes in local magnetization are due to

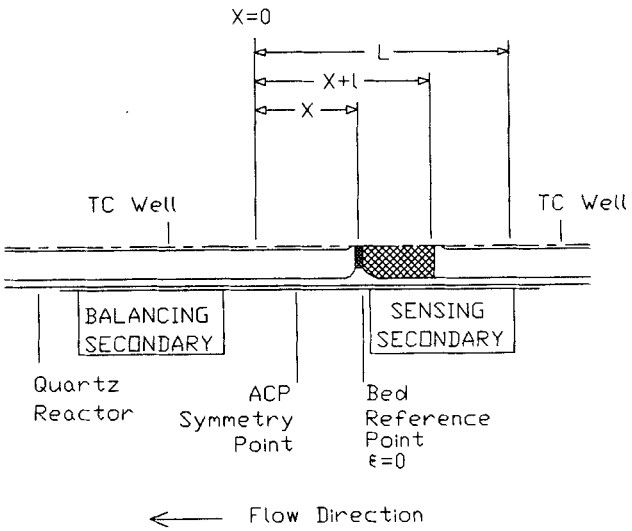

Figure 2. Secondary coils of the ACP and sample.

changes in magnetic field and temperature. Due to the axial symmetry of the coils, no radial information is obtained.

For superparamagnetic samples in a low-intensity AC field, the net magnetization of each catalyst particle (and the entire sample) is small relative to the intrinsic magnetization of the nickel crystallites and follows the applied field. The Langevin low-field approximation for the magnetization of a superparamagnetic specimen (Selwood, 1975) is

$$I(H, T) = \frac{I_\infty(T) I_s(T) \hat{v} H}{3 k_B T} \tag{2}$$

where

H = magnetic field intensity
$I_s(T)$ = intrinsic magnetization of the nickel at temperature T
$I_\infty(T)$ = maximum or saturation magnetization of the sample at temperature T
k_B = Boltzmann's constant
$\hat{v}$ = average volume of the nickel crystallites

While the temperature and field may vary in time and/or space, the average crystallite volume is uniform on a macroscopic scale. There are over ten million crystallites in each cubic micron of the catalyst used in this work. Thus, an averaging volume on the order of a cubic micron is sufficient to define the average properties of the catalyst and be small on the scale of a catalyst particle. Equation 2 applies locally to any such averaging volume.

The sample magnetization at a given bed cross section is proportional to the amount of nickel in that cross section. The local cross-sectional sample saturation magnetization is the local intrinsic magnetization of nickel times the fraction of the coil cross section occupied by nickel. This is expressed as

$$I_\infty(T) = I_s(T) \psi \rho A(\xi) / A_{ccs} \tag{3}$$

where ρ is the local solid fraction in the reactor and ψ is the volume fraction of solid which is nickel. The latter is on the order of 2% and is uniform on a macroscopic scale. The ratio of the local bed cross-sectional area to the coil cross-sectional area completes the specification of the amount of material at ξ. In words, the saturation magnetization is the magnetization which would occur if the moment of every crystallite in the local sample were aligned perfectly with the applied field. This happens only at very high magnetic field intensities, particularly at the high temperatures of concern in this work. Substituting Eq. 3 into Eq. 2, the local magnetization at low field intensity is

$$I(H, T) = \frac{I_s^2(T) \hat{v} \psi \rho}{3 k_B T} (A(\xi)/A_{ccs}) H. \tag{4}$$

Introducing the intensive quantity

$$\Gamma(T) = \frac{I_s^2(T) \hat{v} \psi \rho}{3 k_B T} \tag{5}$$

to represent the temperature dependence of the local sample magnetization, Eq. 1 can be written as

$$E(X, t) = \int_0^\ell \sigma(X + \xi)(A(\xi)/A_{ccs}) \cdot \left\{ H(X, t) \frac{\partial \Gamma}{\partial t} + \Gamma(\xi, t) \frac{\partial H}{\partial t} \right\} d\xi. \tag{6}$$

Assuming that the applied field is spatially uniform within the sensing secondary coil region and is written as

$$H(t) = H_o \sin(2\pi f t) = H_o \sin(\omega t) \tag{7}$$

then Eq. 6 can be written

$$E(X, t) = H_o \int_0^\ell \sigma(X + \xi)(A(\xi)/A_{ccs}) \cdot \left\{ \sin(\omega t) \frac{\partial \Gamma}{\partial t} + \Gamma(\xi, t) \omega \cos(\omega t) \right\} d\xi. \tag{8}$$

The dependence of voltage on X is only through the sensitivity function σ, since temperature is a function of ξ (bed position) and not of X (ACP position) for isothermal coils. The first term in the braces in the integrand in Eq. 8 is the voltage generated by *changes* in temperature. The second term *tracks* the temperature and is much larger in magnitude than the first term for reasonable rates of temperature change. For catalyst temperature profile determinations, the RMS average voltage of Eq. 8 is further averaged over time and recorded at specified positions of the bed in the ACP. As the voltage profiles are measured under steady-state conditions, the first term in braces does not play a role in the analysis. In addition, the constant (in time) value of Γ can be extracted from the RMS averaging process. The ACP voltage recorded with the bed at X_i is

$$V(X_i) = \langle RMS(E(X_i)) \rangle = \int_0^\ell S(X_i + \xi) M(\xi) A(\xi) d\xi \tag{9}$$

where the angle brackets indicate time averaging. The second equality introduces the equation used in profile determinations. The magnitude of the local sample magnetization vector is represented by

$$M(\xi) = \Gamma(\xi) H_o \tag{10}$$

and the ACP's RMS sensitivity is

$$S(X) = \alpha \sigma(X) \omega / A_{ccs} \tag{11}$$

where α is a constant of proportionality. $S(X)$ is the RMS voltage output of the ACP secondary coils due to a reference moment at X, a fixed position in the coils. It has the units of μVRMS/moment. The local moment is expressed as the magnitude of the local magnetization (M) times the differential volume. The units of magnetization are arbitrary since only ratios are currently used in the thermometry. Though the recorded voltage varies in time during reaction initiations and terminations and fluctuates due to noise, time has been dropped from the argument list. This is to emphasize that, during the acquisition of voltage data to be used in the thermometry, the system is at steady state. The origin of the ACP coordinate ($X = 0$) is

assigned to the ACP position for which the value of the integral in Eq. 9 is zero for the bed studied under isothermal conditions. This point is experimentally determined and the outlet face of the catalyst bed is somewhat to the negative of the ACP symmetry point.

Experimental Study

The tubular quartz reactor is designed to allow *in situ* chemisorptive and magnetic catalyst characterizations (Cale, 1984). The bed length of the 170/200-mesh-silica-supported nickel catalyst is 9.0 mm and has a nominal diameter of 11 mm. The top surface of the bed (inlet) is free and the bed rests on a fritted quartz disk. One quartz thermocouple well is centered 1 mm above the free surface to measure the inlet fluid temperature. Another well almost touches the center of the fritted quartz disk which supports the catalyst bed in order to measure the outlet fluid temperature. This catalyst bed, as loaded, has been used extensively in studies of the bed average magnetic thermometry, and both temperature and hydrogen partial pressure calibrations have been established. These calibrations are checked regularly as part of the experimental protocol.

Acquisition of voltage as a function of bed position in the ACP (see Eq. 9 and Figure 2) is started at $X = 0.0$, where the magnetic centroid of the isothermal catalyst bed is at the symmetry point of the secondary coils (see Figure 2). The catalyst is then moved toward the middle of the positive responding secondary coil, with the bed position adjusted manually and read with a resolution of 0.1 mm using a scale built into the height positioner. The ACP voltage is recorded every 2.0 mm in this work. The signal is averaged for 0.6 s by the measuring voltmeter before each value is recorded. These values are further time-averaged to produce the RMS voltage at each coil position. Four sets of voltage vs. bed position in the ACP are then averaged. The reproducibility of voltage at each position of the bed in the ACP depends somewhat on the voltage level, but is less than 3 μVRMS in any case. Errors in positioning add another 5 μVRMS uncertainty to the data in the worst case.

The spatial isothermality limits of the ACP-oven system allowed data to be taken over a length of 36.0 mm (L in Figure 2), before a significant temperature change was noted in the exit fluid temperature. The repeatability of the thermocouple readings is 0.1 K; therefore, a significant temperature change is taken to be 0.2 K. Temporal isothermality is satisfactory, as the temperature of the exit fluid at a given position of the bed is constant beyond the time scale of the experiment. This reflects both the stability of the oven temperature and the steady state of the reactor. The oven is not controlled, as the temperature is more stable with time without the adjustments of a controller.

The established bed average thermometry is part of each experimental sequence in order to compare the average solid temperature to the average calculated from the determined profile. The reaction is initiated with the catalyst positioned at the maximum of sensitivity in the sensing secondary coil ($X = 56$ mm), and the bed average thermometry is performed. After steady state is reached, the reactor is moved to $X = 0.0$ to begin voltage profile measurements. After the voltage vs. position data are taken, the sample is again centered in the positive responding secondary coil. The increase in ACP voltage, after the reaction is stopped, is converted to average temperature decrease. The temperature changes determined in both reaction initiation and termination experiments are the same within experimental repeatability (Cale, 1984). The repeatability of the bed average temperature depends on the thermocouple repeatability, the sample voltage sensitivity, and the noise level during a particular set of experiments. The reproducibility between experiments of the bed average solid temperature, determined using this technique, has been demonstrated to be 0.1 K in favorable cases, limited only by the repeatability of the reference thermocouples. For the catalyst sample studied in this work, the repeatability is 0.2 K. The inlet and outlet fluid temperatures with the bed at $X = 56$ mm are both 0.2 K above those at $X = 0.0$. The higher temperature reflects the small nonisothermality in the oven, and the base (no reaction) temperature is also higher by 0.2 K. Only temperature changes are measured; therefore, the temperature rise above the (local), no reaction temperature will be within the repeatability of the bed average thermometry, independent of bed position between $X = 0$ and $X = 56$ mm.

Calibrations

The magnetochemistry of the ethane hydrogenolysis system can be important; however, it does not play a significant role in the thermometry for the catalyst sample studied. The sample was chosen partly because of its relatively low dispersion, estimated to be 4% from the decrease in ACP voltage upon introducing hydrogen over the fresh catalyst (Cale, 1984; Selwood, 1975). The average crystallite size in the sample depends on the assumptions made in the estimation, but is less than 10 nm. This sample is superparamagnetic at 47 Hz in the operating temperature range of the ethane hydrogenolysis experiments (475–550 K) (Selwood, 1975; Ludlow, 1986). The low dispersion minimizes the impact of changes in hydrogen partial pressure on sample magnetization and any assumptions regarding adsorption. The magnetochemistry of the system is accounted for in profile determinations; however, neither the calibration determination nor its use is discussed.

A calibration relating the local catalyst temperature to the local magnetization is necessary. This calibration is based on a calibration between ACP voltage and bed average temperature, used in the bed average thermometry (Cale, 1984). The calibration between catalyst temperature and ACP voltage is determined in the absence of reaction by changing the sample temperature in a flow of helium. This is done by withdrawing the sample from the oven and then reinserting it to the position which gives the maximum ACP output after the temperature has dropped substantially. The ACP output voltage is followed as the sample reheats. Within several degrees (approximately 20 K) of the oven temperature, the sample temperature changes relatively slowly. In this temperature range, it is assumed that the bed is isothermal and is represented by the exit fluid temperature. The calibration between temperature and voltage is assumed to apply over this limited temperature range. This method gives very reproducible temperature calibrations (Ludlow, 1986). To calibrate over a larger temperature range, the oven temperature is changed and the experiment is done again.

From Eq. 9, the ACP output voltage due to a spatially isothermal bed (T_o) with uniform magnetization (M_o) placed at the value which gives the maximum ACP response for the bed studied ($X = 56$ mm) is,

$$V^m(T_o) = M(T_o) \int_0^\ell S(X + \xi)A(\xi)d\xi. \qquad (12)$$

V^m is used to emphasize that, though the analysis works for an arbitrary X, the data are recorded where the ACP response is maximum. The change in voltage during the reheating is converted to a temperature sensitivity by differentiating Eq. 12 with respect to temperature:

$$\frac{dV^m(T)}{dT} = \frac{dM(T)}{dT}\int_0^{\ell} S(X+\xi)A(\xi)d\xi. \tag{13}$$

Dividing Eq. 13 by Eq. 12, the change in voltage is related to the change in bed moment by

$$\frac{d(M/M_o)}{dT} = \frac{d[V^m(T)/V(T_o)]}{dT}. \tag{14}$$

Equation 14 expresses the linearity of ACP response to magnetic material. The maximum output voltage of the ACP due to the catalyst sample used in this study is 1,940 μVRMS at 524.0 K. The output voltage of the ACP, with the bed at X = 56 mm, changes 16.0 μVRMS/K over a 22 K temperature range (514 to 536 K). Thus, the sample temperature and ACP voltage are linearly related by

$$T = 524.0 + (1{,}940 - V^m)/16.0 = 524.0 - (1{,}940/16.0)(1 - V^m/1{,}940) \tag{15}$$

and the reference temperature and reference magnetization are arbitrary. Equation 15 is used to compute the bed average temperatures from voltage changes. The experimentally-determined temperature dependence of magnetization compares well with past results on nickel catalysts (Cale et al., 1983). Over a larger temperature range, this sensitivity depends on temperature and the reference must be carefully specified.

For nonisothermal beds, a magnetization profile is determined from voltage data by inverting Eq. 9. Then a temperature profile is computed using the experimentally determined temperature dependence of magnetization. The local temperature change is not related directly to ACP voltage change; however, Eq. 15 is still the basis for relating magnetization to temperature. The magnetization ratio

$$r(T, T_o) = M(T)/M(T_o) = M(T)/M_o \tag{16}$$

is introduced to avoid the calculation of absolute values for magnetization. To determine temperature profiles, it is assumed that the temperature dependence of the catalyst's magnetization is spatially uniform. This is true for uniform catalysts and the local temperature is related to the local magnetization ratio through the inverse of Eq. 15:

$$r(T, T_o) = 1 - (16.0/1{,}940)(T - T_o) = 1 - 0.00825(T - T_o). \tag{17}$$

The temperature profile is computed from the magnetization profile using

$$T(\xi) = T_o - (1{,}940/16.0)[1 - r(\xi)] = T_B - (1{,}940/16.0)[r_B - r(\xi)]. \tag{18}$$

The second equality accounts for the fact that the base (no reaction) temperature T_B for a profile determination is not the reference temperature T_o, in general. The magnetization ratio at the base temperature $r(T_B, T_o)$ is calculated using Eq. 17. Because the ACP is linear in sample magnetization, the ratio determined at each cross section is the average moment at that cross section. Since the magnetization is a linear function of temperature, over the limited range of interest, the temperature determined is the cross-sectional average catalyst temperature.

Results and Discussion

In order to determine the magnetization as a function of position in an operating bed, the ACP sensitivity to magnetic material $S(X)$ must be known. This is determined using output voltage vs. catalyst bed position in the ACP obtained on the subject catalyst bed in the absence of reaction at a specific temperature (T_o = 524.0 in this work). The data are obtained after establishing a flow of helium. The magnetization (M_o) of this isothermal reference bed is assumed uniform in the absence of reaction; however, the reactor area decreases somewhat toward the outlet end. Thus, the local cross-sectional moment is not uniform. Measurements of the reactor diameter as a function of bed position are included in the analysis by writing local area as a fraction (f) of the nominal area (A_o). The ACP response due to the catalyst sample with the bed outlet placed at X is then

$$V(X) = M_o A_o \int_0^{\ell} S(X+\xi)f(\xi)d\xi. \tag{19}$$

The sensitivity is determined as a polynomial function of coil position, as

$$S(X) = \sum_{k=0}^{ns} c_k X^k. \tag{20}$$

Then Eq. 19 is

$$V(X) = M_o A_o \sum_{k=0}^{ns} c_k \int_0^{\ell} (X+\xi)^k f(\xi)d\xi. \tag{21}$$

The first term in the sum is a constant, and the corresponding integral represents the constant total volume of the reference bed (divided by A_o). The reference moment and nominal area are included in the sensitivity by defining new coefficients for the polynomial:

$$c'_k = M_o A_o c_k \text{ for } k = 0 \text{ to } ns. \tag{22}$$

So the modified sensitivity

$$S'(X) = \sum_{k=0}^{ns} c'_k X^k \tag{23}$$

depends on the sample, since it depends on sample moment density and sample geometry. Equation 21 can be written as

$$V(X) = \sum_{k=0}^{ns} c'_k \int_0^{\ell} (X+\xi)^k f(\xi)d\xi = \sum_{k=0}^{ns} c'_k \phi_k(X) \tag{24}$$

where ϕ_k replaces the kth integral. The integrals ϕ_k are evaluated using Simpson's (3/8) rule, since f is known at discrete val-

ues of ξ (every 1 mm). The coefficients of the sensitivity polynomial are determined by minimizing the sum of the squares of the differences between the calculated and experimental ACP voltage data over the length of data taken:

$$\underset{\underline{c}}{\text{minimize}}\ Q(\underline{c}) = \sum_{i=1}^{N} [V(X_i) - \sum_{k=0}^{ns} c'_k \phi_k(X_i)]^2 \qquad (25)$$

where N is the number of data points. Coefficient determination is performed using Gauss-Jordan elimination.

The voltage data and resulting sensitivity profile for the bed studied are presented in Figure 3. The sensitivity profile is represented well by a sixth-order polynomial. For convenience, the sensitivity is normalized so that its maximum is unity. Hence, $S'_{max} = M_o A_o$ and a value for M_o is determined in arbitrary units using Eq. 22. M_o represents the magnetization of the sample at 524.0 K. In principle, the normalized sensitivity profiles are applicable to any bed. In reality, they are not expected to be identical because of errors in measuring bed dimensions and perhaps small spatial nonuniformities in catalyst loading. It is, therefore, critical to use the sensitivity profile determined for the same bed for which the temperature profiles are desired in order to account for these small errors. Local magnetization changes on the order of 0.1% are required for temperature profile determinations. Thus, bed measurements would have to be done to that precision in order for the determined sensitivity profile to be universal. Another advantage of the approach taken is that it renders the reference magnetization completely arbitrary as long as the same value is used for operating beds.

In order to determine the temperature profile in an operating reactor, ACP voltages vs. bed position in the ACP are measured after steady state is reached. Two conversion levels are discussed: 1) 11.0% conversion and 2) complete conversion. The no reaction temperature in the 11.0% case is 523.4 K and is 520.6 K for the complete conversion case. These temperatures are different for each other and different from the temperature at which the sensitivity data were taken because of the long-term drift in the oven temperature. The data sets were obtained on different days. The flow rates in both experiments were the same: 26 mL/min STP of hydrogen and 18 mL/min STP of ethane, which corresponds to a Reynolds number of 0.023. The pressure was essentially local atmospheric, as the pressure drop required for this total flow rate is very small.

For the 11.0% conversion level, the average temperature rise above the no reaction reference temperature for the solid is determined to be 5.0 ± 0.2 K using the bed average thermometry. The inlet fluid temperature rise is 0.5 ± 0.1 K, while the outlet fluid temperature rise is 0.9 ± 0.1 K, indicating a considerable amount of axial dispersion and considerable heat loss through the reactor wall. The voltage vs. bed position in the ACP data for this bed are shown in Figure 4. The differences among the voltages at each ACP position and between the isothermal bed and the operating reactor are small relative to the magnitude of the voltages. Nevertheless, the differences are larger than the repeatability of voltage at each ACP position, which is smaller than the size of the data point markers in Figure 4. Since the no reaction base temperature (523.4 K) is lower than the reference temperature (524.0 K), the voltage data from the operating bed cannot be compared directly to that of Figure 3. The magnetization ratio $[r_B = r(T_B, T_o)]$ at the base temperature is greater than 1.

In this work, the magnetization ratio profile is represented as a polynomial in ascending powers of ξ:

$$\frac{M(\xi)}{M_o} = r(T(\xi), T_o) = r(\xi) = \sum_{k=0}^{nm} b_k \xi^k. \qquad (26)$$

This representation was chosen to allow convenient comparison of results with the predictions of a heterogeneous reactor model which uses polynomial approximation (orthogonal collocation); however, the method is limited to cases where the temperature profile can be represented reasonably well by a polynomial. The voltage data can be expressed as

$$V(X) = V^o + M_o A_o \sum_{k=0}^{nm} b_k \int_0^{\ell} f(\xi)\xi^k S(X+\xi)d\xi$$

$$= V^o + M_o A_o \sum_{k=0}^{nm} b_k \Phi_k(X) \qquad (27)$$

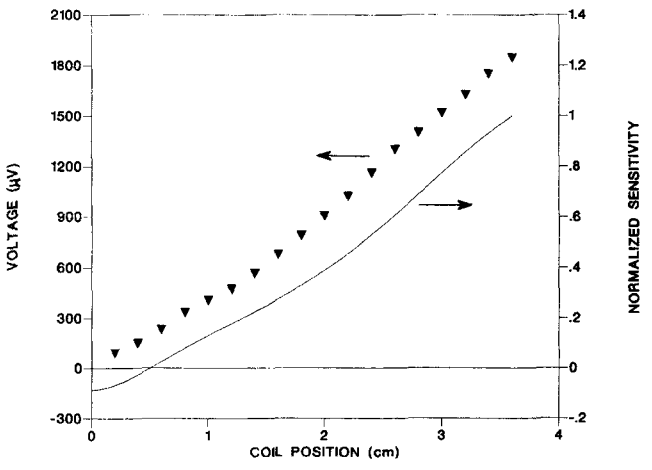

Figure 3. ACP voltage vs. position data for isothermal reactor (T_o = 524.0 K) to determine ACP sensitivity profile.
Uncertainty in the measurements is less than the symbol size.

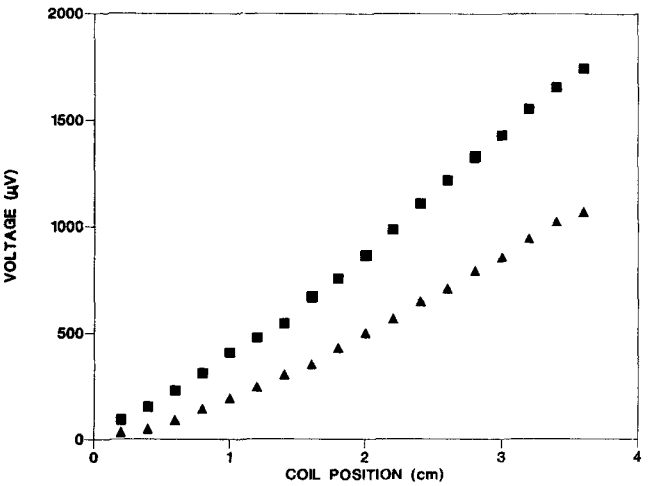

Figure 4. ACP voltage profiles for 11.0% (■) and complete conversion (▲) cases.
Uncertainty in the data is less than the symbol size. Note that the base (no reaction) temperatures are 523.4 and 520.6 K.

where Φ_k, representing the kth integral, is evaluated using Simpson's (3/8) rule. V^o is needed since the integral in Eq. 9 is not zero for an operating, nonisothermal catalyst bed positioned at $X = 0.0$. It is an unmeasurable offset voltage and must be determined as part of the profile determination. Proceeding as for the determination of the sensitivity, $\underline{b}$ and V^o in principle can be determined by minimizing the sum of the squared differences between the data and calculated voltages. Unfortunately, taking this approach is disastrous. Though the back-calculated voltages are very close to the experimental data, the moment profiles are unreasonably wild functions of ξ. The inversion to obtain the magnetization profile is said to be ill-posed, which is a common problem with Fredholm equations of the first kind (Delves and Mohamed, 1985). The difficulty is due to the fact that the kernel of the transformation $[S(X)]$ is "flatter" spatially than the desired function $[M(\xi)]$. Conversely, obtaining $S(X)$ using Eq. 25 posed no difficulty, because the kernel of that transformation $[M(\xi)]$ varied rapidly in space relative to the sensitivity.

"Regularization" is used commonly to deal with the ill posedness of these inversions by incorporating desired properties into the solution (Delves and Mohamed, 1985). In this work, smoothness is introduced into the calculated profile by including a constraint on the variance in the form of a penalty function. The variance is written as:

$$\int_0^\ell [\hat{r} - r(\xi)]^2 d\xi = \int_0^\ell [\ell^{-1} \int_0^\ell r(\xi')d\xi' - r(\xi)]^2 \, d\xi \quad (28)$$

where the bed-average magnetization ratio $\hat{r}$ is calculated from the polynomial (Eq. 26). It is compared with the average magnetization ratio obtained from the bed average thermometry to ensure consistency. V^o and $\underline{b}$ are the solution to:

$$\underset{\underline{b}, V^o}{\text{minimize}} \; Q(\underline{b}, V^o) = \sum_{i=0}^{N} [V(X_i) - V^o - \sum_{k=0}^{nm} b_k \Phi_k(X_i)]^2 + P \int_0^\ell [\hat{r} - r(\xi)]^2 \, d\xi. \quad (29)$$

Gauss-Jordan elimination is used to determine the solution. The difficulty is choosing a value for P. If P is too large, the resulting moment profile will be uniform at the average, while if P is too small the profile obtained will vary wildly.

The value of P is determined from extensive trial calculations. A catalyst temperature profile is assumed, which is converted to magnetization profile via Eq. 17. $V(X)$ "data" are generated using the established sensitivity, $S(X)$. Many different "data" sets are generated by adding noise to each point using a random number generator (Rice, 1983) and then truncating to represent experimental data. The noise is added so that the resulting variation in the generated "data" corresponds to the experimental level. A magnetization, hence temperature, profile is then calculated for each of the noisy "data" sets using Eq. 29. The results of thousands of these inversions are analyzed for a range of P values. For each value of P, this procedure gives an approximately Gaussian distribution of temperatures at each bed position. The average at each cross section is the most probable temperature, with the standard deviation of the distribution being a measure of the uncertainty.

The value of P, for which the calculated local average temperature is the input temperature, increases with the uncertainty in the data. Over a substantial range in values for the penalty above the minimum, the average temperature profile is essentially the input profile. At very large values of P, the average temperature at each point is pulled toward the *bed-average* temperature. In the range of penalty values which allows back calculation of the input profile, the standard deviation of the temperature distribution at each bed position decreases with increasing P. The value of P chosen is the highest value which does not cause a noticeable difference between the input temperature profile and the calculated profile.

Figure 5 displays the temperature profile for the 11.0% conversion case, calculated from the experimental data using the value of P determined. To verify that the value of P used did not distort this specific profile, it was used as the starting profile and the trial calculations discussed above were repeated. The solid temperature profile in Figure 5 is based on a fifth-order polynomial, because there is no significant difference between it and a sixth-order polynomial. The solid temperature increases about 0.5 K through the bed and the inlet solid temperature is about 4.5 K above the no reaction temperature. The calculated most likely solid temperature goes through a slight maximum, and its derivative at the outlet is close to zero. It is reassuring that the experimentally-based profile supports the corresponding result (or assumption) found commonly in heterogeneous reactor modeling (Khanna and Seinfeld, 1987; Odendaal et al., 1987). The calculated profile indicates an average solid temperature rise of 4.9 K above the no reaction base temperature. The bed average temperatures computed during the trial calculations are within the ±0.2 K experimental repeatability of the bed-average thermometry for the vast majority of the random distributions of noise added and for any value of P which allowed meaningful profiles to be calculated. This reflects the experimentally-established reproducibility of 0.2 K in the bed-average thermometry.

The local temperatures fall within the bounds shown in Figure 5 in 68% and 95% of the inversions. The bounds were computed every 1.0 mm, and the lines are present to guide the eye. The percentages correspond to one and two standard deviation units of a normal distribution. The predicted solid temperature at the bed inlet is within ±0.29 K and ±0.56 K of the most likely inlet temperature for 68% and 95% of the trial computations.

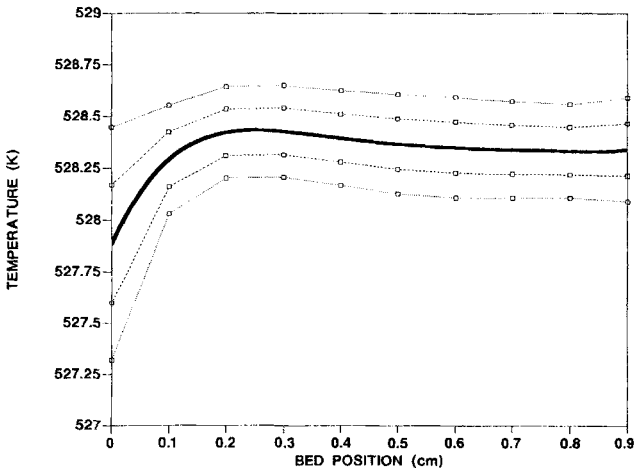

Figure 5. Temperature profile for 11.0% conversion experiment, using a fifth-order polynomial.

The plot is from reactor inlet to outlet, which corresponds to plotting the profile from $\xi = \ell$ to $\xi = 0$. The 68% and 95% certainty levels are also shown.

The reliability is considerably better in the majority of the bed, as the temperature is likely to be within ±0.13 K and ±0.25 K of the local average for the listed percentages. The uncertainty in the profile increases toward the inlet of the bed because the remainder of the bed is so close to the same (and average) temperature. Thus, the random noise introduced into the "data," during the trial calculations, is disproportionately accounted for by adding variance to the magnetization at the bed inlet. A higher value of P narrows the distribution of temperatures about the local average and tends to pull the local average temperature to the bed average. This skewing effect of P is noted first at the bed inlet ($\xi = \ell$), again because the average temperature is largely determined by the majority of the bed. Computations using trial temperature profiles which are smoother spatially show that the uncertainty is distributed more uniformly over the bed and is about 0.2 K at the 95% level. Such temperature profiles would occur at the same conversion level at higher Reynolds numbers, since the decreased effect of axial dispersion in the fluid would result in a lower inlet solid temperature. The 11.0% conversion case, *as run,* is a good test of the magnetic determination of solid temperature profiles, with a relatively small change in temperature occurring over a short length of reactor.

In order to obtain complete conversion at the same flow rates as for the 11.0% conversion case, the hydrogen flow was reduced until the average solid temperature started increasing dramatically and then reset. Experimentally, the inlet fluid temperature rise above the no reaction condition is 18.5 K, while the temperature rise of the exit fluid is 10.4 K. Considerable axial dispersion is apparent, in addition to significant radial heat loss. ACP voltage data for the complete conversion case, shown in Figure 4, reflect a large increase in bed temperature. The average temperature rise above the no reaction base temperature, based on Eq. 15, is 47 K. The calculated average of close to 570 K is well outside of the range of validity of the calibration. Since the temperature sensitivity of the magnetization increases (in absolute value) toward the Curie temperature, this is a lower bound on the average temperature increase. Indeed, attempts to determine the magnetization profile indicate that the catalyst at the reactor inlet is nonmagnetic; i.e., above the Curie temperature of 627 K. Qualitatively, the complete conversion case represents the upper steady-state solution to the diffusion-reaction problem in the pellets at the inlet conditions. It is clear that the thermometry is only useful over temperature ranges where calibrations are available and certainly below the Curie point of the magnetic material. This is not a severe limitation, as materials which are both superparamagnetic and catalytic are available over a very wide temperature range (Kittel, 1976).

The potential to use well-defined cross-sectional average solid temperature profiles for heterogeneous model development and parameter estimation is clear. The results of the 11.0% conversion case demonstrate that the uncertainties in local solid temperatures depend on the profile determined. Trial calculations indicate that a 0.25 K to 0.5 K uncertainty (at the 95% level) in local solid temperatures for profiles at higher conversions can be expected with the current equipment and experimental protocol. Higher conversions, which have larger spatial temperature variations, are therefore expected to provide significantly better relative precision. Higher conversion cases will also require more extensive computations, since a high-order polynomial may be needed to represent the temperature profile. This affects both the solid temperature profile and the model parameter estimations. Alternative functional forms can be used in such cases. The conversion level can be chosen to balance uncertainty in local temperature values and computational difficulties, since model parameter values should be conversion-independent.

Model simulations are needed to determine the precise dependence of the uncertainties in parameter value estimates on the uncertainties in local solid temperatures; however; improved reliability in temperatures will improve parameter estimates. Trial calculations using the temperature profile of Figure 5 indicate that the uncertainty throughout the bed would be within the current 0.1 K thermocouple repeatability with an improvement of a factor of ten in signal to noise ratio. A similar improvement in precision can be realized by decreasing the spatial scale of the ACP secondary coils in order to reduce the difficulty with the inversion of the Fredholm equation (Eq. 29) (Wing, 1985). Equipment and protocol are being developed to achieve this increased precision.

As there is no other method to measure cross-sectional average solid temperature, validation of the magnetic temperature profile determinations will come through experiments on systems for which there are established correlations for model parameters. For example, experiments at higher Reynolds numbers and with larger catalyst particle sizes will allow comparison of predicted parameter values with the accepted values for specific models (Froment and Bischoff, 1979). Experiments designed to optimize the prediction of specific parameters can also be developed. Thermocouple-measured temperatures of larger catalyst particles may allow pointwise comparison with magnetically-determined solid temperature profiles. Comparing point values with cross-sectional averages will at least provide a consistency check, though the interpretation of thermocouple-measured temperatures is subject to debate.

Acknowledgment

We gratefully acknowledge support of this project by the National Science Foundation, grant CBT-8711452.

Notation

A = area, cm^2
b = coefficients in the polynomial for magnetization profile
c = coefficients in the polynomial for sensitivity profile
c' = modified coefficients in the polynomial for sensitivity profile
E = instantaneous voltage output of ACP with the bed at position X
f = ratio of local cross-sectional area to nominal area
H = magnetic field strength, Oe
I = magnetic moment density, arbitrary units
k_B = Boltzmann's constant
ℓ = length of catalyst bed, cm
L = range of X over which data was taken, cm
M = magnitude of the magnetic moment density, arbitrary units
N = number of data points for regression
ns = order of polynomial representing sensitivity
nm = order of polynomial representing moment density profile
P = penalty for variance constraint
Q = objective function for determination of coefficient vectors
r = ratio of local magnetization to reference magnetization
S = ACP sensitivity to a unit moment at a given position, μVRMS/moment
T = temperature, K
t = time, s
V = recorded time average RMS voltage, μV
$\hat{v}$ = average nickel crystallite volume, nm^3
X = position of bed reference point relative to its starting value, cm

Greek letters

α = constant of proportionality
ξ = coordinate for bed position relative to the quartz frit, cm
ϕ = integral introduced in Eq. 24
Φ = integral introduced in Eq. 27
ψ = fraction of solid which is nickel
ρ = solid fraction in each cross section
Γ = dimensionless quantity introduced in Eq. 5
σ = output voltage of ACP per unit rate of change of magnetization
ω = frequency of excitation voltage

Subscripts

B = no reaction state
o = sensitivity data and conditions thereof
i = index for data points
k = index for the polynomial terms
s = spontaneous or intrinsic
∞ = saturation or infinite field
ccs = coil cross section

Superscripts

o = voltage at $X = 0$ for nonisothermal beds, μVRMS
m = indicating maximum in voltage
$'$ = modified constants for sensitivity profile

Literature Cited

Balakrishnan, A. R., and D. C. T. Pei, "Heat Transfer in Gas-Solid Packed Bed Systems: 1. A Critical Review," *Ind. Eng. Chem. Process Des. Dev.*, **18**(1), 30 (1979).

Cale, T. S., "Effectiveness Factor for a Single Pellet During Ethane Hydrogenolysis," *Chem. Eng. Comm.*, **70**, 57 (1988).

———, "Nickel Crystallite Thermometry During Ethane Hydrogenolysis," *J. Cat.*, **90**(1), 40 (1984).

Cale, T. S., and J. M. Lawson, "Application of Catalytic Crystallite Thermometry to Interphase Transport Studies," *Chem. Eng. Comm.*, **39**, 241 (1985).

Cale, T. S., J. M. Lawson, and D. K. Ludlow, "Low Re Interphase Nu for Axial Dispersion and Bypassing Reactor Models," *Chem. Eng. Comm.*, **56**, 169 (1987)

Cale, T. S., and D. K. Ludlow, "Magnetic Crystallite Thermometry," *J. Cat.*, **86**(2), 450 (1984a).

———, "Application of AC Permeametry to Catalytic Crystallite Thermometry," *Anal. Inst.*, **13**(2), 183 (1984b).

Cale, T. S., J. T. Richardson, and J. Ginestra, "Size Effect on Magnetic Moment Density of Dispersed Nickel," *App. Phys. Lett.*, **42** (8), 744 (1983).

Delves, L. M., and J. L. Mohamed, *Computational Methods for Integral Equations*, Cambridge University Press, Cambridge (1985).

Froment, G. F., and K. B. Bischoff, *Chemical Reactor Analysis and Design*, Wiley, New York (1979).

Hayt, W. H., *Engineering Electromagnetics*, 3rd ed., McGraw-Hill, New York (1974).

Holstein, W. L., and M. Boudart, "The Temperature Difference between a Supported Catalyst Particle and its Support During Exothermic and Endothermic Catalytic Reactions," *Rev. Latinoam. Ing. Quim. Quim. Apl.*, *13* (**2**), 107 (1983).

Khanna, R., and J. H. Seinfeld, "Mathematical Modeling of Packed Bed Reactors: Numerical Solutions and Control Model Development," *Advances in Chemical Engineering*, **13** (1987).

Kehoe, J. P. G., and J. B. Butt, "Interactions of Inter- and Intraphase Gradients in a Diffusion Limited Catalytic Reaction," AIChE J., **18**, 347 (1972).

Kittel, C., *Introduction to Solid State Physics*, 5th ed., Wiley, New York (1976).

Ludlow, D. K., "The Application of Magnetic Crystallite Thermometry to Low Reynolds Number Interphase Heat Transfer," PhD Dis., Arizona State Univ. (1986).

Luss, D., "Temperature Rise of Catalytic Supported Crystallites," *Chem. Eng. J.*, **1**(4), 331 (1970).

Odendaal, W., W. Gobie, and J. J. Carberry, "Thermal Parameter Sensitivity in the Simulation of the Nonisothermal, Nonadiabatic Fixed Bed Catalytic Reactor—The Two Dimensional Heterogeneous Model," *Chem. Eng. Comm.*, **58**, 37 (1987).

Rice, J. R., "Numerical Methods, Software, and Analysis, IMSL Reference Edition," McGraw-Hill, New York (1983).

Richardson, J. T., "Sulfiding of Nickel Catalyst Beds," *J. Cat*, **21**(1), 130 (1971).

Selwood, P. W., *Chemisorption and Magnetization*, Academic Press, New York (1975).

Sharma, S., D. Boecker, G. J. Maclay, and R. D. Gonzalez, "The Simultaneous Measurement of Support, Metal, and Gas Phase Temperatures Using an *in Situ* IR Spectroscopic Technique," *J. Cat.*, **110**, 103 (1988).

Steinbruchel, Ch., and L. D. Schmidt, "Heat Dissipation in Catalytic Reactions on Supported Crystallites," *Sur. Sci.*, **40**, 693 (1973).

Wing, G. M., "Condition Numbers of Matrices Arising from the Numerical Solution of Linear Integral Equations of the First Kind," *J. Integ. Eq.*, **9**(suppl.), 191 (1985).

Manuscript received Feb. 7, 1989, and revision received June 21, 1989.